Assembling Native Elementary Cellulose Nanofibrils via a Dynamic and Spatially Confined Functionalization

Marco Beaumont,[1#] Blaise L. Tardy,[2#] Guillermo Reyes,[2] Tetyana V. Koso,[4] Elisabeth Schaubmayr,[1] Paul Jusner, [1] Alistair W. T. King,[3] Raymond R. Dagastine,[4] Antje Potthast,[1] Orlando J. Rojas,[2,5]* and Thomas Rosenau[1,6]**

[1] Department of Chemistry, Institute of Chemistry for Renewable Resources, University of Natural Resources and Life Sciences Vienna (BOKU), Konrad-Lorenz-Straße 24, A-3430 Tulln, Austria.

[2] Department of Bioproducts and Biosystems, School of Chemical Engineering, Aalto University, P.O. Box 16300, Espoo FI-00076, Finland.

[3] Materials Chemistry Division, Department of Chemistry, University of Helsinki, AI Virtasen aukio 1, FI-00560 Helsinki, Finland.

[4] Department of Chemical & Biomolecular Engineering; The University of Melbourne, Victoria, Australia.

[5] Bioproducts Institute, Department of Chemical & Biological Engineering, Department of Chemistry and department of Wood Science, 2360 East Mall; Chemistry, 2036 Main Mall, and Wood Science, 2424 Main Mall, The University of British Columbia, Vancouver, BC V6T 1Z3, Canada.

[6]Johan Gadolin Process Chemistry Centre, Åbo Akademi University, Porthansgatan 3, Åbo/Turku FI-20500, Finland.

[#]These authors contributed equally to this work. *Corresponding authors: thomas.rosenau@boku.ac.at, orlando.rojas@ubc.ca, marcobeaumont1@gmail.com

KEYWORDS: Individualized nanofibers, reversible succinylation, nanocellulose processing, TEMPO-oxidation, functional biocolloids, imidazole chemistry

Abstract

Selective surface modification of bio-sourced colloids affords effective fractionation and functionalization of polysaccharide-based nanomaterials, as shown by the classic TEMPO-mediated oxidation. However, such route leads to changes of the native surface chemistry, affecting interparticle interactions and limiting the full exploitation of the supermaterial properties associated with such nanomaterial assemblies. Here we introduce a methodology to extract elementary cellulose fibrils by treatment of biomass with *N*-succinylimidazole, achieving spatially confined (92% regioselectivity towards primary C6-OH) and dynamic surface functionalization, as elucidated by nuclear magnetic resonance, infrared spectroscopy, and gel permeation chromatography. No polymer degradation or crosslinking nor changes in crystallinity occur under the mild conditions of the process yielding elementary fibrils. The structure of the fibrils was validated by cross-corelating solid-state NMR, chromatographic analysis, and atomic force microscopy imaging. We demonstrate the fully reversible nature of the dynamic modification, which offers a significant opportunity for the reconstitution of the interfaces back to the native states, chemically and structurally. Consequently, access to 3D structuring of native elementary cellulose I fibrils is made possible, reproducing the supramolecular features of the native cellulosic supermaterials. Overall, we propose the reversible and regioselective surface succinylation as a suitable route to overcome current limitations in the production of cellulose nanomaterials, which is required to unlock the full potential of cellulose as a sustainable building block.

New bio-based feedstock streams are needed to develop sustainable materials that surpass in performance the prevalent synthetic counterparts. In this regard, the isolation from biomass of native structural components of high intrinsic cohesion and defined morphology presents a unique opportunity.[1] The biogenesis of cellulose chains from synthase systems results in polymeric constructs with the highest strength reported to date. Driven by supramolecular interactions, tightly packed elementary fibrils are formed (diameter of approx. 3-4 nm) exhibiting a remarkable tensile strength and modulus, reaching values as high as 7 GPa[2,3] and 140 GPa,[4–6] respectively. They can be readily obtained from forestry, ocean and agricultural side-streams and their promise in high-performance sustainable materials has triggered great interest over the last decade.[1,3] However, there is a standing need for new, green routes to re-engineer the native cellulosic supramolecular interactions into macroscale materials, ideally in line with green chemistry and technology principles.

Mechanical fibrillation of the plant cell wall, following optional pretreatments (*e.g.*, enzymatic), results in bundled of cellulose nanofibrils (CNFs) carrying residual hemicelluloses, which dominate most supramolecular interactions, given their higher surface activity and reactivity.[7,8] The most prominent chemical pretreatment that enables individualization into elementary fibrils is a regioselective modification by oxidation of the cellulose's primary OH groups, namely, TEMPO-mediated oxidation (2,2,6,6-tetramethylpiperidin-1-yl-oxyl being the oxidant).[9] An alternative approach is the periodate oxidation and subsequent Pinnick oxidation,[10] which converts the secondary alcohol groups of cellulose into carboxyl moieties. While these modifications are commonly used, they also present major drawbacks, including those related to chemical degradation and their irreversibility. For instance, complete surface modification of the nanofibrils by TEMPO-oxidation has been demonstrated to occur in alkaline media,[11,12] causing a drastic decrease in molar mass,[13] even observed after moderate oxidation conditions (in the range of 0.5 mmol COOH g^{-1} of CNFs).[14,15] These effects limit the mechanical performance and the corresponding prospects of the assembled materials.[16] In addition, TEMPO-oxidation is irreversible, yielding nanofibrils with carboxylated surfaces, which prevent the strong interactions that is otherwise present in the native supramolecular structures.[11] By contrast, cellulose esters can be cleaved by saponification, enabling the recovery of the intrinsic surface functionality and cohesive interactions.[17] This latter observation inspired our inquiries, as presented in this discussion.

Herein, cellulose fibers were deconstructed into elementary fibrils by regioselective modification with *N*-succinylimidazole (**Figure 1**). This surface modification is introduced on the entire fibril surface, with very high selectivity towards the primary hydroxyl group of cellulose.[18–20] The method is mild and does not lead to dissolution nor influence the inherent physico-chemical properties such as crystallinity, and molar mass while preserving the morphology of the elementary, even at complete surface functionalization. Preserving such native properties are essential to maintain the excellent mechanical properties of cellulose.[4,5] The negative carboxylate charge facilitates individualization into elementary nanofibrils, which can be processed, in a similar fashion as TEMPO-CNF, into an arbitrary shape, e.g. via extrusion, wet-spinning or film formation.[1,21,22] Although for TEMPO-CNF the interfacial interactions were impacted by carboxyls groups, the succinyl ester moieties can be hydrolyzed (saponified) under basic conditions to recover the pristine chemical structure of cellulose I, re-accessing its native supramolecular interactions. This offers a unique route to enhance processability of plant biomass into materials while recovering their performance potential. We describe the efficiency of the reaction, its regioselectivity, and reversibility by nuclear magnetic resonance, infrared spectroscopy, and gel permeation chromatography. The morphology of the elementary fibrils is then evaluated using atomic force microscopy and scanning electron microscopy, revealing the fibril morphology and size, which match that of the native fibrils. Finally, we demonstrate processing in aqueous media that leads to hydrogels, aerogels and films, the latter being compared for their mechanical properties before and after saponification. The introduced, new avenue to engineer cellulosic building blocks will unlock new opportunities in the fabrication of sustainable, high strength and light-weight materials.

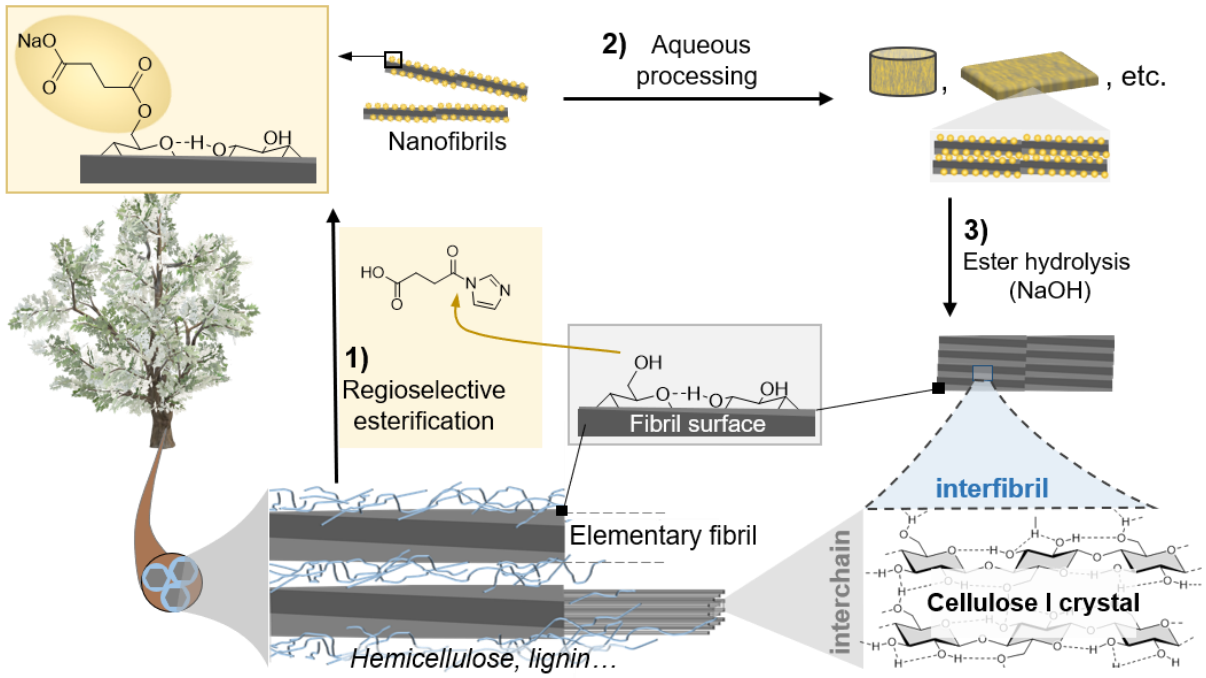

Figure 1. Elementary succinylated cellulose nanofibrils (C6SA-CNF) were produced from renewable cellulose fibers by regioselective esterification of the primary C6-OH by reaction with *N*-succinyl imidazole followed by fibrillation in a high-pressure homogenizer (1). As is the case of conventional CNF, C6SA-CNF forms hydrogels of given shapes (2) but is amenable to removal of the installed groups by facile hydrolysis. Hence, 3D structures can be formed by the elementary fibrils of cellulose in its type I, the native cellulose allomorph (3). The hydrolysis treatment induces strong interfibrillar interactions, rivaling those present in the native cellulose I crystals.

Results and Discussion

The preparation of structural assemblies based on pristine individualized cellulose nanofibrils is shown schematically in **Figure 1**. The native cellulose fibers were regioselectively modified by succinylation of the surface C6-OH glucose repeating units. Thereby, CNF with the same selectivity (C6) and largely similar chemical functionality (succinate vs.carboxylate) as the well-known TEMPO-CNF were obtained. The esterification was mediated *via* a reactive acylimidazole intermediate,[18–20] and can be applied directly to never-dried biomass, *i.e.,* wet pulp fibers, commonly used for the preparation of typical CNF .[10,12,18] as it is an acyl transfer rather than a classical esterification mechanism.

The modification proceeded in an acetone/water solvent system in the presence of succinic anhydride (1.0 molar equivalents based on cellulose monomer unit) and imidazole (1.5 equivalents) that react *in situ* to form *N*-succinylimidazole (**Figure 2A**). The esterification was completed after approx. 6 h, but we note that the final carboxylate content can be tailored by varying the reaction conditions (**Figure S1**). Successful introduction of the succinyl group was demonstrated by infrared spectroscopy, which confirmed the presence of the carbonyl bands at 1568 cm^{-1} and 1723 cm^{-1} (**Figure 2B**). The modified cellulose was directly compared with the starting material, never-dried cellulose fibers, which is referred to as 'reference'. The degree of substitution, determined by conductometric titration (**Figure S2**) was 0.25 ± 0.02, corresponding to a carboxylate content of 1.3 ± 0.1 mmol/g (**Table S1**). These values were also confirmed by diffusion-edited liquid state NMR in the $[P_{4444}][OAc]$:DMSO-d_6 solvent.[23,24] This analysis also afforded information on the regioselectivity of the modification (**Figure 2C**),[19,20] and NMR peaks were assigned through the respective multiplicity-edited heteronuclear single-quantum correlation (HSQC) spectrum (**Figure S3**). The calculated total DS and that specific to the primary C6-OH were 0.24 and 0.22, respectively, yielding a reaction regioselectivity of 92%. Based on the crystallite size, we calculated the theoretically available number of C6-OH (**Table S1**), and concluded that the entire number of available C6-OH groups at the surface of the elementary fibrils was modified, which has been so far only possible by severe TEMPO-oxidation.[11] Solid-state NMR (**Figure S4** and **Figure 2E**), was used to gather information on the fibril superstructure based on deconvolution of the C4 peak, composed of a chemically non-accessible, crystalline core, and an accessible surface.[25,26] One of the peaks corresponding to the chemically accessible surface - shaded in dark grey and bronze for reference and C6SA-CNF, respectively - is clearly shifted upfield (from 83.2 ppm to 82.5 ppm) upon surface modification. We assign this peak to C4 of the C6-succinylated glucopyranose surface units and further derive a homogeneous surface modification. In addition, it is clearly shown that the fibril superstructure and crystallinity (**Table S1**) is well preserved, and contrasts with NMR results of TEMPO-oxidized CNF (**Figure S5**). Compared to oxidative treatments, such as periodate or TEMPO-oxidation, the molar mass is not reduced (although changes occurred due to the introduction of succinyl groups, **Figure 2D**). The increase of the weight-averaged molar mass upon modification (**Table S2**) is the result of removal of

hemicelluloses and/or low molar mass cellulose fractions; the former possibility, in fact, was confirmed by solid-state NMR measurements (**Table S1**).

The effect of the fibrillation degree on the rheological properties was assessed for C6SA-CNF and compared to that of TO-CNF (prepared under neutral conditions)[14] (**Figure S6**), showing that C6SA-CNF underwent a slightly more extensive fibrillation. Moreover, we show that as other CNF types, C6SA-CNF exhibits strong shear-thinning and the rheological properties typical of a gel, due its dominating elastic behavior (G' > G'') (**Figure S7**).

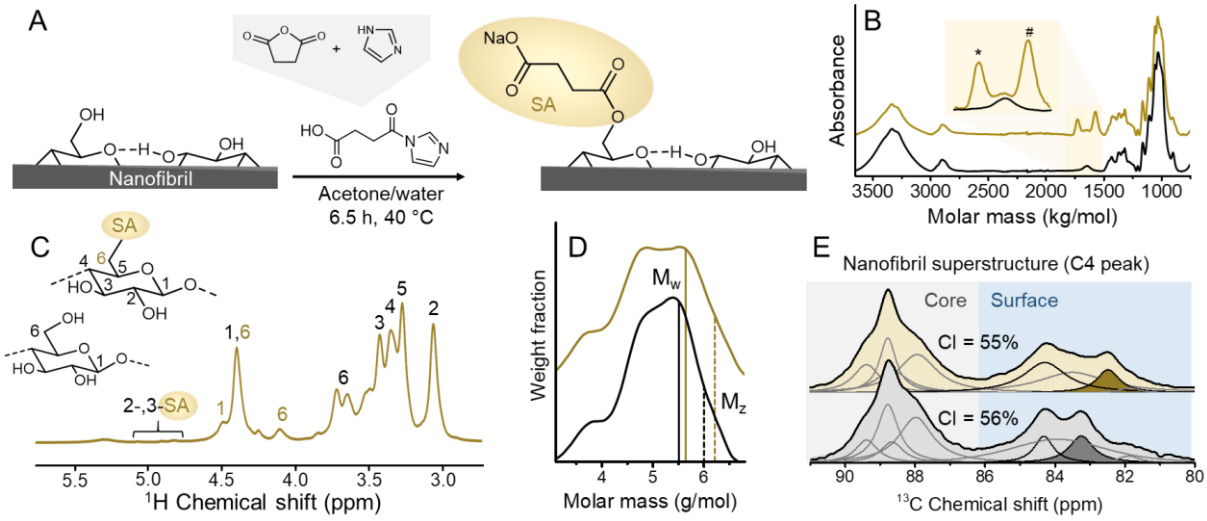

Figure 2. *N*-Succinyl imidazole, the acyl transfer agent, was produced *in situ* through reaction of imidazole and succinic anhydride (A). The wet cellulose fibers were esterified at 40 °C for 6.5 h in an acetone/water mixture to introduce the succinyl group onto the primary C6-OH of cellulose (92% selectivity). The IR spectrum clearly demonstrates the successful introduction of the succinyl group (* λ = 1723 cm^{-1}, # λ = 1568 cm^{-1}) (B) and the regioselectivity was studied by solution-state nuclear magnetic resonance, showing only minor modification of the C2- and C3-OH (C). The molar mass (both weight- and z-averaged) increased through introduction of the succinyl group (D). The superstructure and crystallinity index (CI), studied by solid-state NMR, was preserved, confirming that the reaction was confined to the accessible (amorphous) nanofibril surface (E).

The morphology and dimensions of the nanofibrils were evaluated using atomic force microscopy (**Figure 3**). When observed, in the given scanning areas, that the fibrils appeared rather homogeneous (**Figure 3A**); meanwhile, the absence of bundling suggested complete individualization into elementary nanofibrils through our process.

Figure 3A includes over 50 fibrils that were clearly individualized and the corresponding height profiles revealed rather uniform height values across the sample (**Figure 3A2**), *e.g.,* a narrow height distribution (3.4 nm ± 0.6 nm, **Figure S9**). These values agree with those measured for elementary fibrils (also referred to as crystallite size) of approx. 4 nm (**Table S1**). This clearly indicates a complete fibrillation of the cellulose fiber into its elementary nanofibrils. Interestingly, a small fraction of the deposits on the surface were smaller fibrils with heights below 1 nm and lengths of ca. 20 nm. These may be cellulosic fragments resulting from the pulping process, fibrillation treatment and/or residual hemicelluloses.

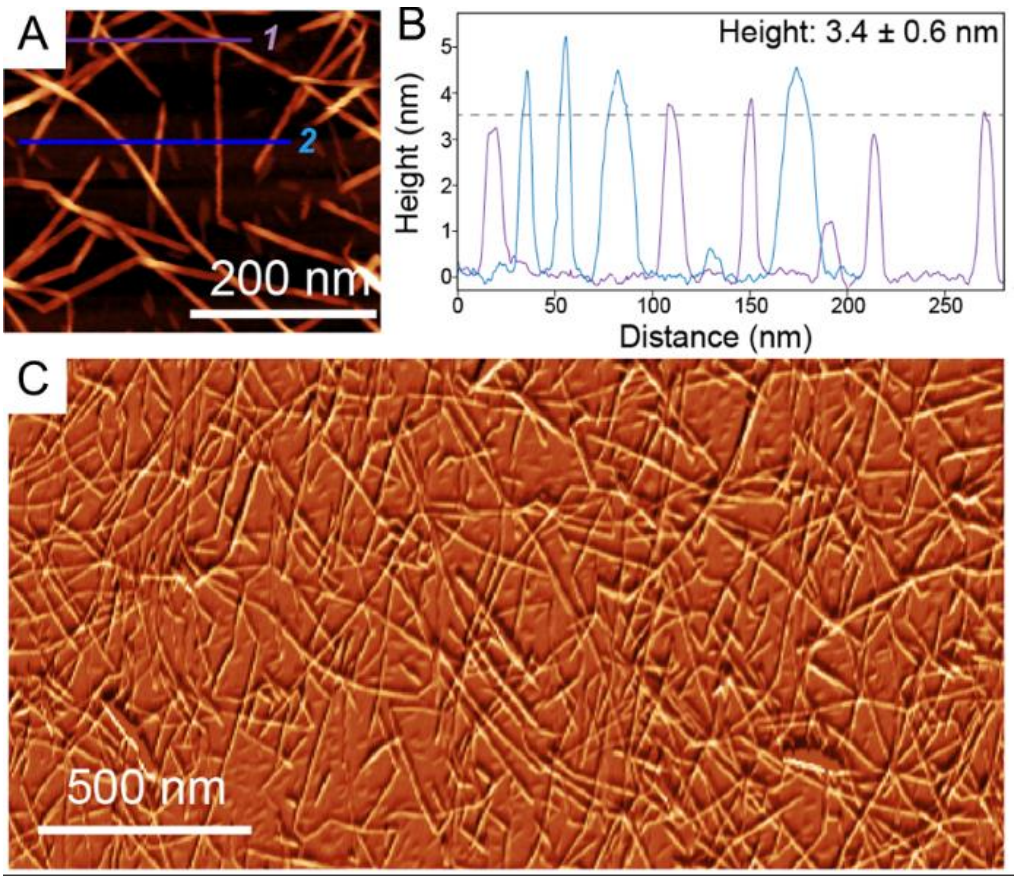

Figure 3 (A) Atomic force microscopy imaging of elementary fibrils of C6SA-CNF and (B) height profiles obtained for 9 fibrils. (C) The overview microscopy image indicates well dispersed and homogeneous fibrils (C).

The chemistry used herein is nondestructive, which contrasts significantly with the oxidative routes conventionally used for modification or enhanced dispersion of nanocelluloses. Moreover, the introduced succinate ester is stable under conventional conditions (pH range 3-9). This enables a wide and versatile application range for

C6SA-CNF. It is well known that ester groups are susceptible to hydrolysis, *i.e.,* saponification. This is applicable to our modified CNF, *i.e*., by treatment with 0.1 M NaOH, yielding native elementary CNF, which we submit to be similar to the natural form (herein referred to as *nat*-CNF) (**Figure 4A**). It can be reasonably proposed that pristine cellulose is restored after hydrolysis, upon removal of the succinate groups, as demonstrated by IR spectroscopy (**Figure 4B**) through the disappearance of the carbonyl bands and as also shown by gel permeation chromatography with multi-angle light scattering detection. Both weight- and z-average molar mass of the succinylated cellulose were clearly reduced upon saponification, returning to values similar to those of the reference sample, which is also well reflected in the respective molar mass distributions (**Table S2** and **Figure S8**). Moreover, the conformation plot of *nat*-CNF (**Figure 4C**) showed that after hydrolytic treatment the shape and dependency of the radius of gyration and molar mass of the dissolved cellulose sample, returned to the initial, reference state. Generally, the alkaline treatment induced a crosslinking/gelation of the C6SA-CNF, similar to the behavior of carboxylated CNF under acidic conditions (protonation) or in presence of multivalent ions (ionic crosslinking through replacing Na^+ counterion).

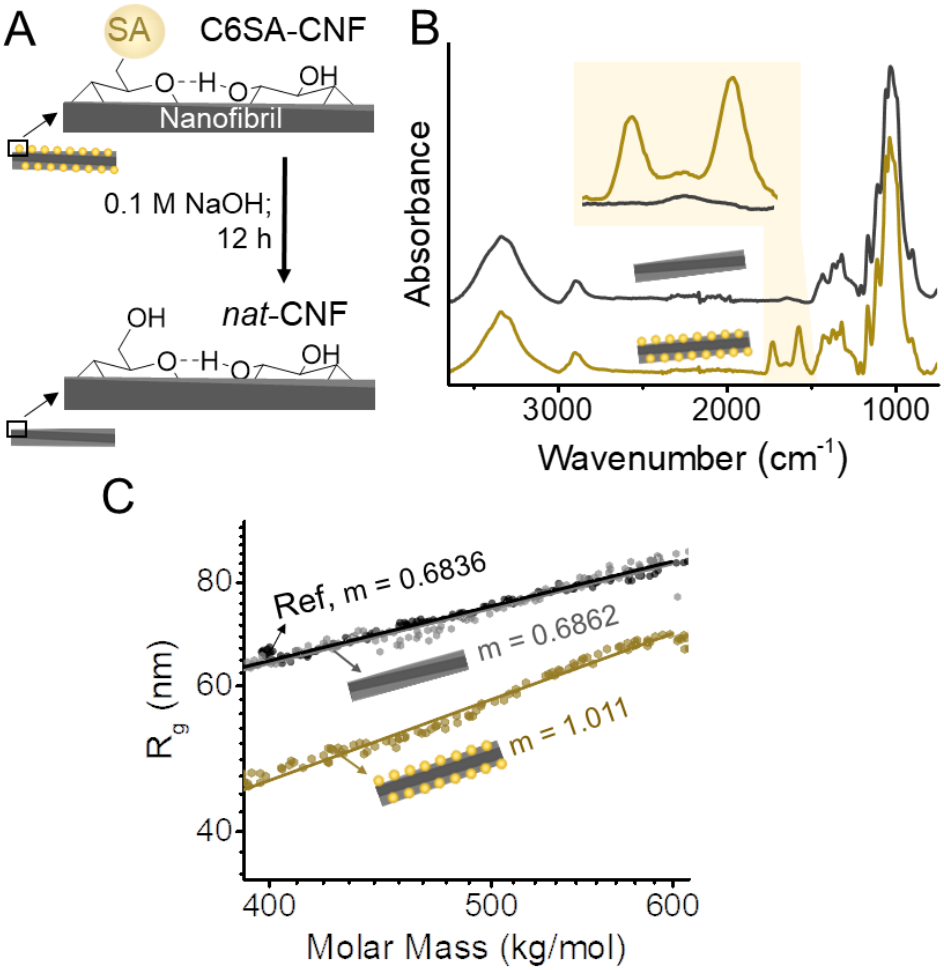

Figure 4. (A) Regioselective introduction of succinyl groups in C6SA-CNF (top-left) can be reversed by alkaline treatment (0.1 M NaOH, bottom-left), as shown by IR spectroscopy, through the disappearance of the carbonyl bands (B), as well as by the conformation plot from light scattering analysis (C). The conformation plot (molar mass vs. radius of gyration, R_g) of the NaOH-treated C6SA-CNF and its slope (m) is almost identical compared to the native sample (Ref), confirming the reversible nature of the esterification.

The alkaline treatment can be conducted directly from C6SA-CNF in sodium form, or C6SA-CNF hydrogels prepared by ionic crosslinking. The properties of swollen networks of C6SA-CNF and TO-CNF, both processed into films, were then evaluated as a function of the conditions of the aqueous suspension (**Figure S10**). The films were swollen to equilibrium under various conditions and evaluated through the increase in thickness in relation to the dry film. In pure water, both C6SA-CNF and TO-CNF films swelled significantly, as shown by the 8.5- and 15-fold increase in thickness, respectively. The lower increase of C6SA-CNF is most probably related to the fact that

the succinyl groups of C6SA-CNF are less hydrophilic compared to the carboxylate groups in TO-CNF. In contrast, the thickness increased significantly less in mild acidic conditions (0.01 M HCl), due to the protonation of the carboxylate groups and thereby induced gelation (due to lower electrostatic repulsion). In comparison, upon exposure to a base treatment (0.1 M NaOH), the thickness of TO-CNF films increased to a similar level as that in pure water (13-fold), while C6SA-CNF swelling was severely limited (3-fold), which is a result of the ester hydrolysis into *nat*-CNFs and the induced gelation.

The mechanical properties of the hydrogels (measured while immersed in the respective aqueous solution) were evaluated by tensile testing, **Figure 5A-B**, with representative tensile strain curves shown in **Figure 5C**. As expected, both TO-CNF and C6SA-CNF hydrogels showed a rather low mechanical strength when immersed in water, 0.3 and 2.2 MPa, respectively. The results are in line with the lower swelling of C6SA-CNF, which helps to resist the effect of water in the wet conditions. C6SA-CNF and TO-CNF films presented similar tensile strengths under acidic conditions, 12.5 and 20 MPa, respectively (**Figure S11**); the elastic modulus and toughness followed similar ranking. Upon 0.1 M NaOH treatment, the mechanical properties of the TO-CNF hydrogel were similar to those measured in water. In contrast, the tensile strength of NaOH-treated C6SA-CNF (*nat*-CNF, **Figure 5B**) were of the same order as that of C6SA-CNF, 12 MPa, when the aqueous medium was changed to an acid medium (**Figure S11**). This demonstrates that the ester hydrolysis (saponification) induced physical crosslinking, due to the removal of the charged ester group, restoring the hydrogen-bond network of native celluloses. The hydrogels were solvent-exchanged with acetone and supercritically dried and the resultant nanofibrillar network was observed by scanning electron microscopy. The network formed showed similar structures prior to and after removal of the succinyl groups. We speculate that the network formed after saponification resembles that of native cellulose nanofibrils (**Figure 5D-E**).

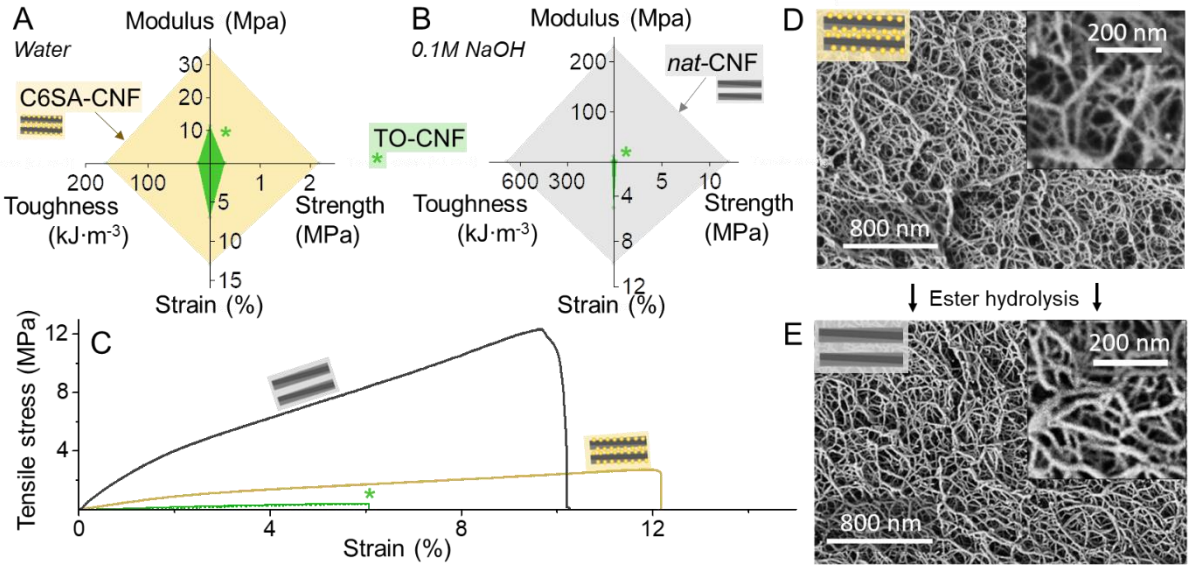

Figure 5 Mechanical performance of hydrogels produced from C6SA-CNF and TO-CNF, which were equilibrated in water prior (B) and after (A) treatment in 0.1M NaOH. C6SA-CNF exhibits stronger mechanical stability in water, which is especially pronounced in case of prior NaOH treatment, causing ester hydrolysis to yield *nat*-CNF. (C) Representative tensile profiles of the systems compared in A and B. Networks of C6SA-CNF (D) and *nat*-CNF (E) in an aerogel. The schematic figures highlight the possible nanofiber surface structure with and without prior NaOH treatment.

As shown in **Figure 5a3,** the supramolecular interactions in water, upon recovery of the native cellulose interfaces, resulted in an improved tensile strength, by ca. 6-fold, with a relatively small reduction of the strain at break, from 13% to 10%. By favoring supramolecular interactions, upon drying, the strain at break was on the other hand reduced, from 3.2% to 1.8% (**Figure 6**). The mechanical performance of the respective dry films are compared in **Figure 6**. A significant increase in strength (a 2.5-fold increase, from 79 MPa to 194 MPa) was realized. Likewise, the moduli increased from 7.9 GPa to 19.4 GPa. This suggests that a significant improvement in the interfacial cohesion results from the recovery of the native supramolecular interactions, after saponification. With increased anisotropy, *i.e.,* with increased coherence between the fibrils, one can expect further increase in strength of the formed films.

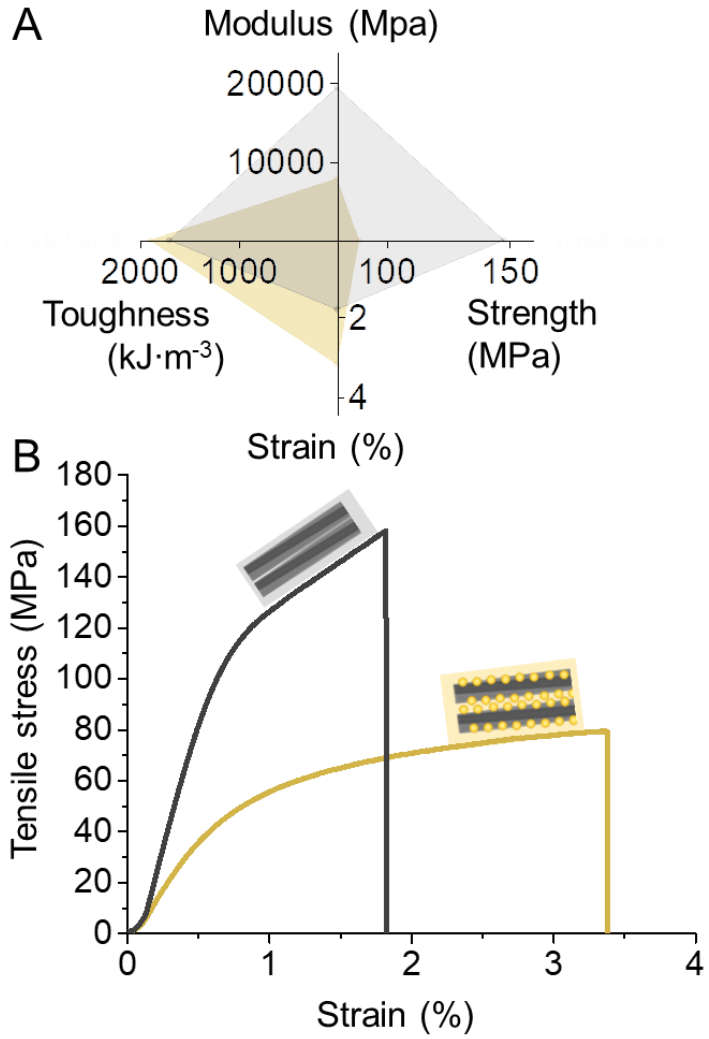

Figure 6 (A) Mechanical properties of dried, isotropic films of C6SA-CNF (yellow profile and shade) and nat-*CNF* (grey profile and shade). (B) Representative stress-strain curves for the samples indicate the suggested recovery of the native, interfibrillar cohesion of nat-*CNF*.

In conclusion, we have shown that our aqueous-based succinylation enables complete isolation of the elementary fibrils from wood fibers, without compromising the crystalline structure and degree of polymerization, within and on the surface of the nanofibrils. Moreover, we show that the proposed modification enables complete esterification of the available primary hydroxyl groups of the elementary fibril, *i.e.* full surface coverage, and thereby fibrillation into elementary nanofibrils. The resulting nanofibril dispersions could be processed using conventional approaches while making possible restoration of the native supramolecular interactions, by following a mild hydrolysis (saponification). The reversibility of the proposed functionalization enables structures comprising elementary nanofibrils exhibiting their more

characteristics, which can overcome the current limitations in mechanical performance of nanocelluloses. Structures composed of native elementary cellulose fibrils, made available by our approaches, is expected to further the developments and implementation of materials from sustainable building blocks. We expect that the introduced methods will push the upper strength boundaries measured for nanocelluloses, and their implementation in a wider range of applications.

References

[1] B. L. Tardy, B. D. Mattos, C. G. Otoni, M. Beaumont, J. Majoinen, T. Kämäräinen, O. J. Rojas, *Chem. Rev.* **2021**, in revision.
[2] T. Saito, R. Kuramae, J. Wohlert, L. A. Berglund, A. Isogai, *Biomacromolecules* **2013**, *14*, 248–253.
[3] T. Li, C. Chen, A. H. Brozena, J. Y. Zhu, L. Xu, C. Driemeier, J. Dai, O. J. Rojas, A. Isogai, L. W\aagberg, *Nature* **2021**, *590*, 47–56.
[4] I. Diddens, B. Murphy, M. Krisch, M. Müller, *Macromolecules* **2008**, *41*, 9755–9759.
[5] I. Sakurada, Y. Nukushina, T. Ito, *J. Polym. Sci.* **1962**, *57*, 651–660.
[6] A. Šturcová, G. R. Davies, S. J. Eichhorn, *Biomacromolecules* **2005**, *6*, 1055–1061.
[7] B. D. Mattos, B. L. Tardy, O. J. Rojas, *Biomacromolecules* **2019**, *20*, 2657–2665.
[8] X. Yang, M. S. Reid, P. Olsén, L. A. Berglund, *ACS Nano* **2019**, *14*, 724–735.
[9] A. Isogai, L. Bergström, *Curr. Opin. Green Sustain. Chem.* **2018**, *12*, 15–21.
[10] S. F. Plappert, J.-M. Nedelec, H. Rennhofer, H. C. Lichtenegger, F. W. Liebner, *Chem. Mater.* **2017**, *29*, 6630–6641.
[11] Y. Okita, T. Saito, A. Isogai, *Biomacromolecules* **2010**, *11*, 1696–1700.
[12] Y. Kobayashi, T. Saito, A. Isogai, *Angew. Chem. Int. Ed.* **2014**, 10394–10397.
[13] T. Saito, S. Kimura, Y. Nishiyama, A. Isogai, *Biomacromolecules* **2007**, *8*, 2485–2491.
[14] T. Saito, M. Hirota, N. Tamura, S. Kimura, H. Fukuzumi, L. Heux, A. Isogai, *Biomacromolecules* **2009**, *10*, 1992–1996.
[15] T. Saito, M. Hirota, N. Tamura, A. Isogai, *J. Wood Sci.* **2010**, *56*, 227–232.
[16] Z. Fang, B. Li, Y. Liu, J. Zhu, G. Li, G. Hou, J. Zhou, X. Qiu, *Matter* **2020**, *2*, 1000–1014.
[17] S. W. Pattinson, A. J. Hart, *Adv. Mater. Technol.* **2017**, *2*, 1600084.
[18] M. Beaumont, S. Winklehner, S. Veigel, N. Mundigler, W. Gindl-Altmutter, A. Potthast, T. Rosenau, *Green Chem.* **2020**, *22*, 5605–9.
[19] M. Beaumont, P. Jusner, N. Gierlinger, A. W. T. King, A. Potthast, O. J. Rojas, T. Rosenau, *Nat. Commun.* **2021**, *12*, 2513.
[20] M. Beaumont, C. G. Otoni, B. D. Mattos, T. V. Koso, R. Abidnejad, B. Zhao, A. Kondor, A. W. T. King, O. J. Rojas, **2021**, DOI 10.26434/chemrxiv.14401712.v1.
[21] N. Mittal, F. Ansari, K. Gowda.V, C. Brouzet, P. Chen, P. T. Larsson, S. V. Roth, F. Lundell, L. Wågberg, N. A. Kotov, L. D. Söderberg, *ACS Nano* **2018**, *12*, 6378–6388.
[22] M. Beaumont, A. Potthast, T. Rosenau, in *Cellul. Sci. Technol.* (Eds.: T. Rosenau, A. Potthast, J. Hell), John Wiley & Sons, Inc., Hoboken, NJ, USA, **2018**, pp. 277–339.

[23] T. Koso, D. Rico del Cerro, S. Heikkinen, T. Nypelö, J. Buffiere, J. E. Perea-Buceta, A. Potthast, T. Rosenau, H. Heikkinen, H. Maaheimo, A. Isogai, I. Kilpeläinen, A. W. T. King, *Cellulose* **2020**, *27*, 7929–7953.
[24] A. W. T. King, V. Mäkelä, S. A. Kedzior, T. Laaksonen, G. J. Partl, S. Heikkinen, H. Koskela, H. A. Heikkinen, A. J. Holding, E. D. Cranston, I. Kilpeläinen, *Biomacromolecules* **2018**, *19*, 2708–2720.
[25] K. Wickholm, P. T. Larsson, T. Iversen, *Carbohydr. Res.* **1998**, *312*, 123–129.
[26] X. Nocanda, P. T. Larsson, A. Spark, T. Bush, A. Olsson, M. Madikane, A. Bissessur, T. Iversen, *Holzforschung* **2007**, *61*, DOI 10.1515/HF.2007.095.

Supporting Information

Table S1. Physical properties of the native cellulose fibers and succinylated C6SA-cellulose.

	Reference	C6SA-Cellulose
Weight-averaged molar mass, M_w (kg/mol)	321	421
Z-averaged molar mass, M_z (kg/mol)	999	1641
Weight-averaged degree of polymerization (DP)	1982	2203
Crystallite size (nm)*	4.1	4.1
Crystallinity (%)*	55.6%	55.4%
Hemicellulose content (%)*	2.3%	1.4%
Degree of substitution (DS) (mmol/mmol)	-	0.25,[#] 0.24[§]
DS (C6OH) (mmol/mmol)	-	0.22[§]
Accessible primary hydroxyl groups (mmol/mmol)[&]	0.21	0.22

*Calculated from the deconvoluted solid-state spectra, shown in **Figure 2e**. DS was measured by conductometric titration[#] and liquid-state NMR[§]. [&]Accessible primary hydroxyl groups per cellulose monomer unit was calculated from the crystallite size, according to Okita *et al*.[12]

Table S2. Physical properties of the native cellulose fibers and succinylated C6SA-cellulose.

	Reference	C6SA-Cellulose	Hydrolyzed C6SA-Cellulose
M_w (kg/mol)	321	421	355
M_z (kg/mol)	999	1641	1027
Weight-averaged DP	1982	2203	2189

Table S3. Reaction conditions in the optimization of the succinylation at a reaction temperature of 40 °C and 1.0 Eq. (molar equivalent based on glucose monomer unit) succinic anhydride. The influence on the DS was estimated from the intensity of the IR carbonyl band at 1730 cm^{-1}.

Run	Imidazole (Eq.)*	Reaction time (h)	IR carbonyl (a.u.)
1	1.3	0.25	0.12
2	1.5	3.25	0.127
3	1.1	6.25	0.133
4	1.3	6.25	0.132
5	1.1	3.25	0.121
6	1.5	0.25	0.115
7	1.5	6.25	0.136
8	1.3	3.25	0.12
9	1.1	0.25	0.117
10	1.3	3.25	0.121
11	1.3	3.25	0.128
12	1.3	3.25	0.119
13	1.3	3.25	0.12
14	1.3	3.25	0.123
15	1.3	3.25	0.122
16	1.5	6.25	0.133
17	1.1	3.25	0.123
18	1.3	0.25	0.112
19	1.1	6.25	0.129
20	1.5	0.25	0.117
21	1.5	6.25	0.136
22	1.1	0.25	0.113

*Equivalents based on glucose monomer unit.

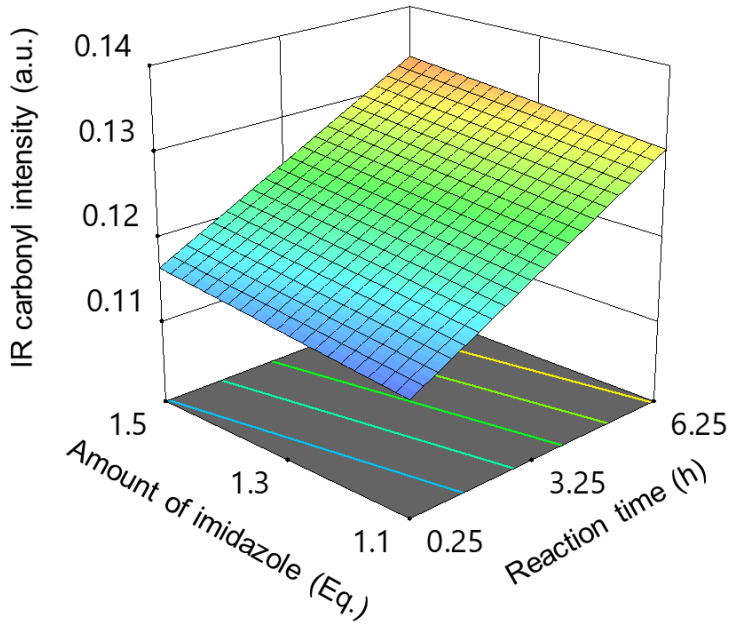

Figure S1. The influence of Factor **A**, the amount of imidazole (molar equivalents based on glucose monomer unit) and Factor **B**, reaction time, in reactions with 1.0 Eq. of succinic anhydride, acetone/water as solvent and a temperature of 40 °C. The model equation from the optimization is $IR\ carbonyl\ intensity = 0.103667 + 0.008077\boldsymbol{A} + 0.002872\boldsymbol{B}$. The infrared (IR) carbonyl intensity corresponds to the final DS (intensity of 0.134 approximates a DS of 0.25) and the equation can be used to finetune the DS of the C6SA-cellulose.

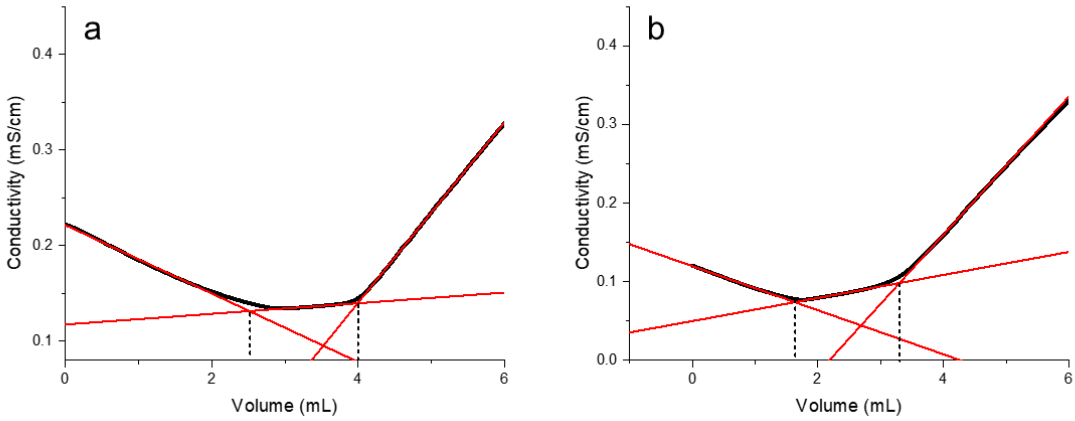

Figure **S2**: Conductivity titrations of freeze-dried C6SA-CNF with 10 mM HCl to determine the degree of substitution (0.25) and carboxylate content (1.3 mmol/g) from the plateau of the curves.

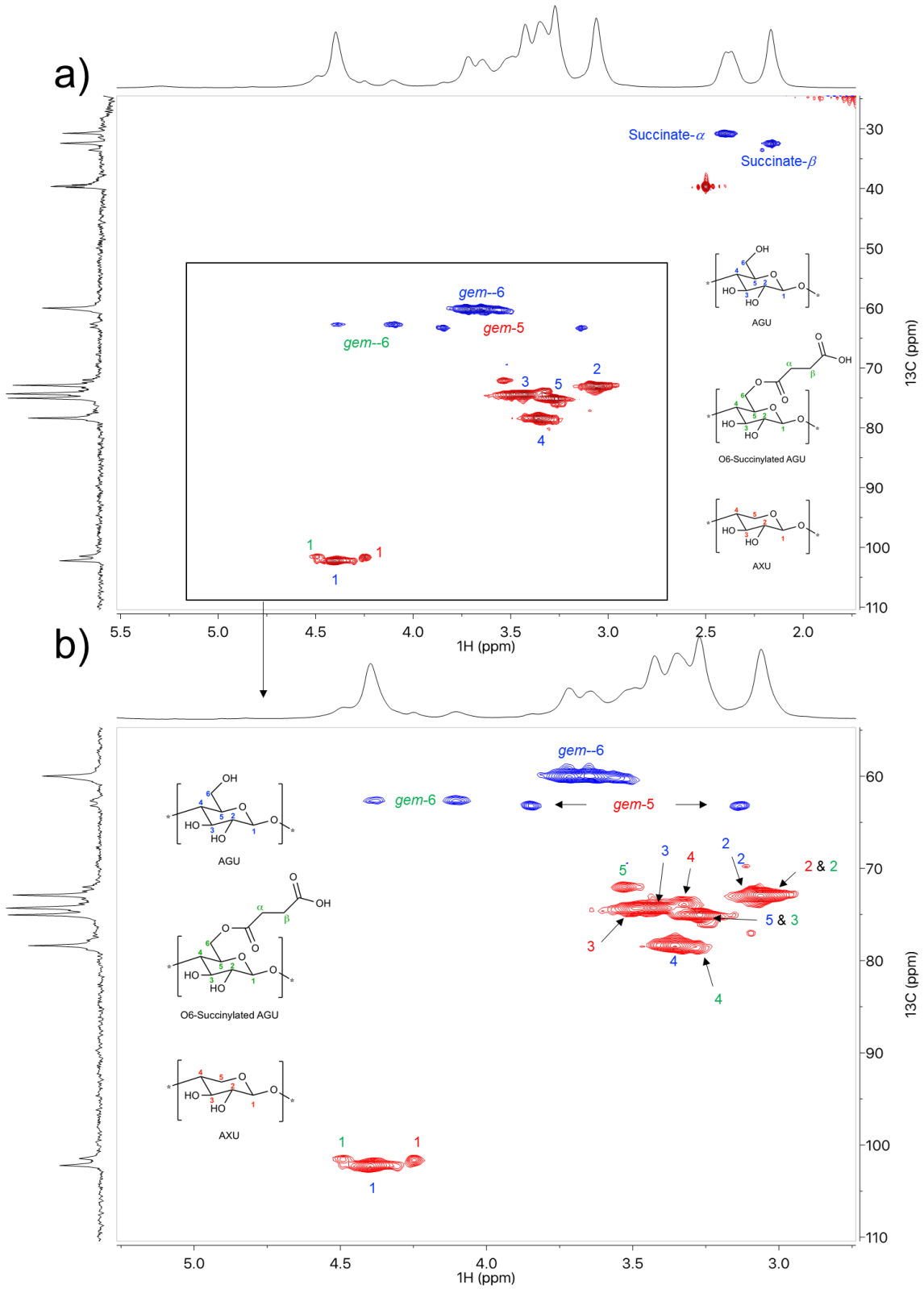

Figure **S3**: Multiplicity-Edited heteronuclear single-quantum correlation (HSQC) 2D NMR spectrum (a) and zoom (b), including the peak assignments of native cellulose (nanofibril core), succinylated cellulose (nanofibril surface) and hemicellulose traces (xylan).

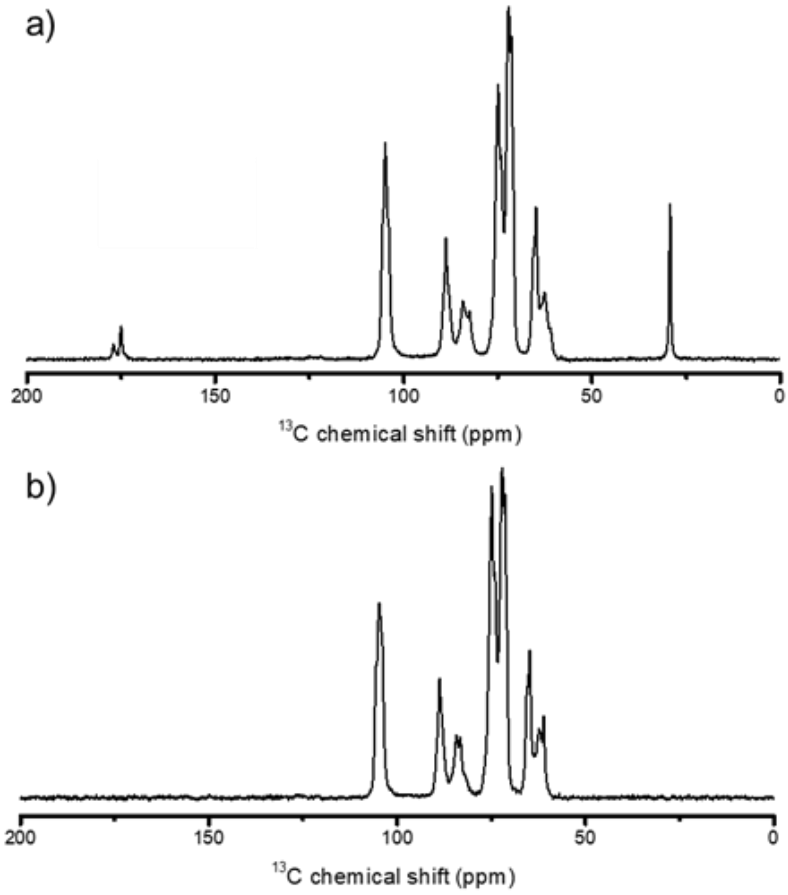

Figure S4: Solid-state NMR of C6SA-cellulose (a) and the native cellulose fibers (reference, b).

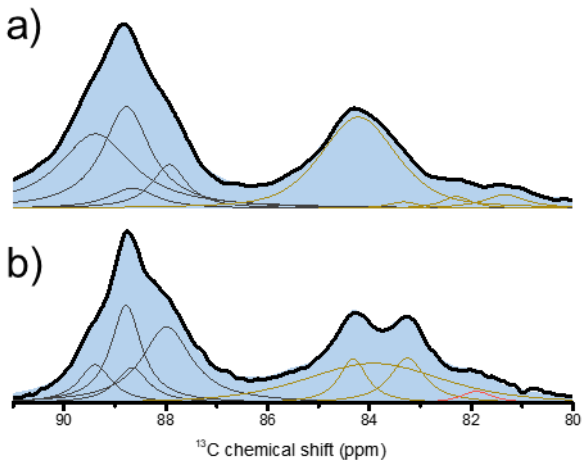

Figure S5: Deconvoluted C4 peak of the solid-state NMR of TEMPO-oxidized cellulose in comparison to the native starting material.

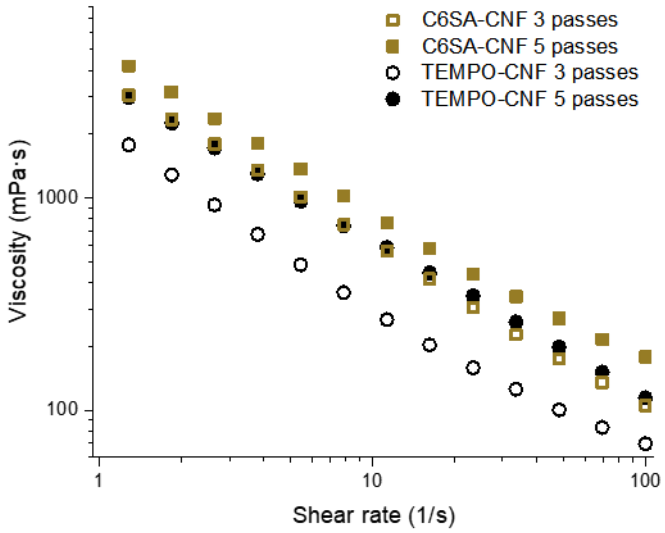

Figure S6: Influence of the number of passes through a high-pressure homogenizer on the viscosity of C6SA-CNF in comparison to TEMPO-CNF.

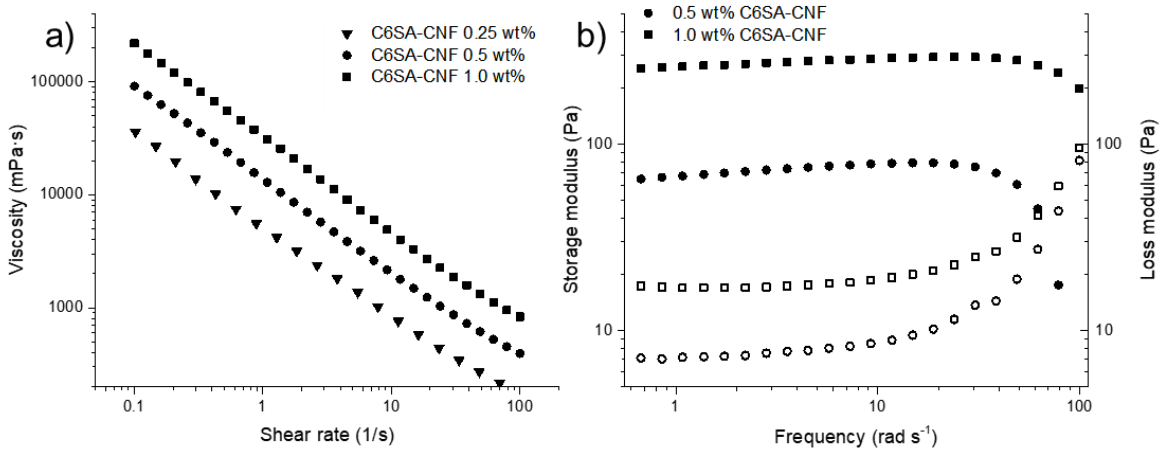

Figure S7: Rheological properties of individual C6SA-CNF dispersion. Viscosity vs. shear rate (a) and shear moduli vs. frequency (b).

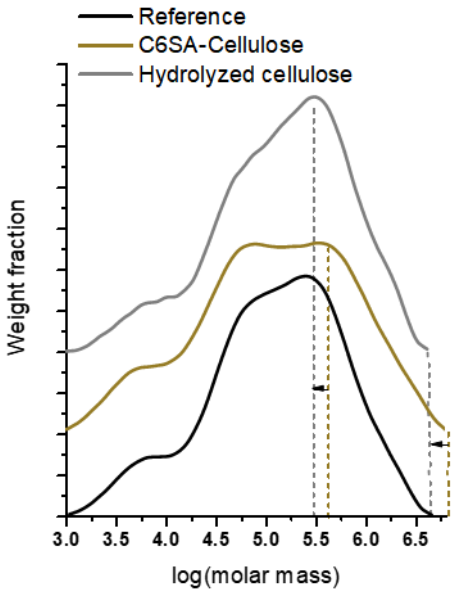

Figure S8: Molar mass distributions of reference sample, succinylated cellulose (C6SA-cellulose) and pristine sample, after basic hydrolysis (hydrolyzed cellulose). The shift of the chromatogram to lower mass values (indicated with black arrow) from C6SA-cellulose to hydrolyzed cellulose is a further indication of the successful removal of the succinate group.

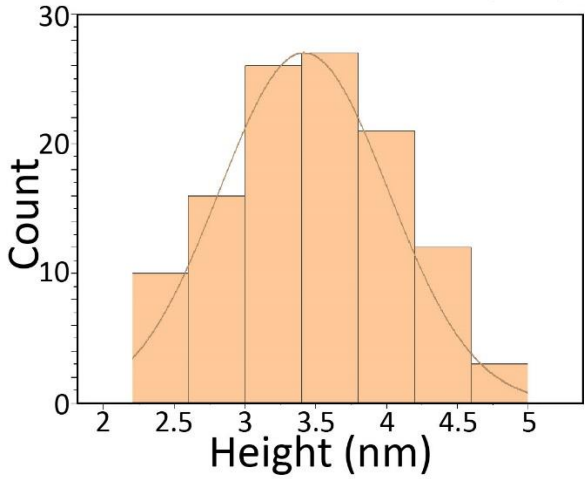

Figure S9: Distribution of height from C6SA-CNF.

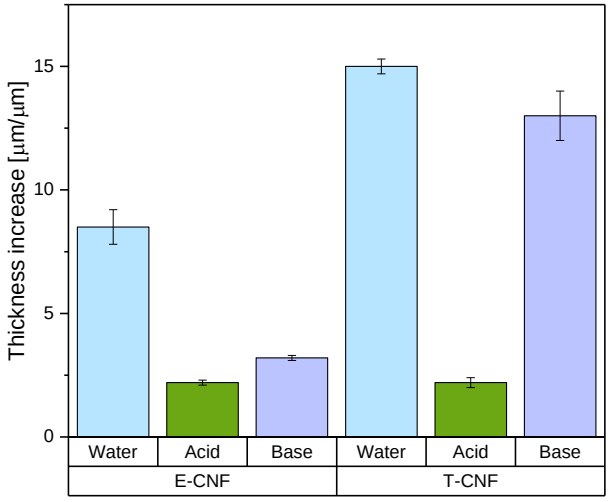

Figure S10: Swelling of C6SA-CNF and TO-CNF as a function of the aqueous medium, measured by the thickness increase of prepared nanofilms.

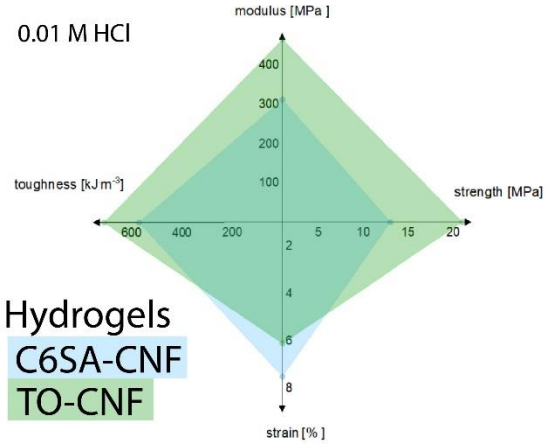

Figure S11: Tensile properties of hydrogels of C6SA-CNF and TO-CNF in their protonated state.

Materials and Methods

Cellulose fibers of high purity were provided as never-dried bleached beech sulfite dissolving pulp (50 wt% solid content) by Lenzing AG (Lenzing, Austria) and used in the production of the esterified pulp sample (C6SA-Cellulose). All chemicals were purchased from Sigma-Aldrich (Merck Life Science OY, Finland) at minimum purity of 99% and were used as received.

Optimization of the succinylation reaction

The reaction optimization was performed with the program Design-Expert Version 11 from Stat-Ease, Inc (Minneapolis, Minnesota, USA) was used. Previously, screening tests were performed to identify the model limits for the optimization: amount of imidazole (1.0-1.5 Eq. based on glucose monomer unit) and reaction time (0.25 h – 6.25 h). The optimization was performed with a randomized, quadratic response surface type of model and a set of experimental conditions was predicted (Table SXX). As response values, IR analysis was performed and the carbonyl band at 1730 cm^{-1} was selected to predict the amount of introduced succinate at the respective reaction conditions.

Preparation of regioselectively succinylated cellulose nanofibrils (CNFs)

Never-dried cellulose fibers (20.0 g wet mass, 10 g dry mass, 61.7 mmol, 50 wt% solid content) was transferred into a flask. In a separate container, 30.8 mL of a 3 M solution of imidazole (6.30g, 92.5 mmol, 1.5 molar equivalents) in acetone were stirred with 61.7 ml of a 1 M succinic anhydride solution (6.17 g, 61.7 mmol, 1.0 molar equivalents) in acetone for 10 min. Afterwards this mixture was added to the cellulose fibers, and mixed homogeneously by stirring with a glass rod for 1 min. The container was closed and heated in an oven at 40 °C for 6.25 g. The reaction was stopped through addition of a saturated solution of $NaHCO_3$ in deionized water and 30 min equilibration. To remove the unreacted SA and the imidazole from the cellulose, the pulp was washed by filtration with deionized water. The cellulose fibers were suspensed in deionized water at 0.25 wt% solid content with a blender.

C6SA-cellulose suspension was fibrillated in a high-pressure homogenizer, the Gaulin APV-1000 from AxFlow GesmbH (Premstätten, Austria). The homogenization of the fibers was done in 5 passes at pressure of approx. 800 bar to yield a highly viscous and transparent dispersion of C6SA-CNF.

Preparation of TEMPO-oxidized CNF (TO-CNF)

TO-CNF were prepared according to a procedure from the literature.[1] Never-dried cellulose fibers (20 g, 10 g dry mass) was suspended in 0.05 M sodium phosphate buffer (900 mL, pH 6.8), TEMPO catalyst (0.016 g, 0.1 mmol) and sodium chlorite (80%, 1.13 g, 10 mmol) were added under stirring. A 2 M sodium hypochlorite solution (5 mL, 10 mmol) was diluted to 0.1 M in 0.05 M sodium phosphate buffer and was added to the reaction mixture. The flask was immediately stoppered, and the suspension was stirred at 500 rpm and 60 °C for a designated time (48 h). After cooling the suspension to room temperature, the TEMPO-oxidized celluloses were thoroughly washed with deionized water by filtration. The fibers were dispersed at a solid content of 0.25 wt% and the pH was adjusted to 8 to deprotonate the carboxyl groups. Finally, the fibrillation was conducted using the same conditions as in case of C6SA-CNF.

Conductometric titration: To determine the degree of substation and carboxylate content. For the titration 10.9 mg of freeze-dried C6SA-CNF was dissolved in 30 ml of deionized water. Then 4 ml of a 0.01 M NaOH solution was added, and the mixture was stirred until the conductivity value was constant. The titration was done with a Metrohm 856 Conductivity Module using a Mettler Toledo Seven Easy Conductivity Electrode (Greifensee, Switzerland). During the titration, a total of 8 ml 0.01 M HCl was added in 0.05 ml steps. The plateau in the titration curve (**Figure SXX**) was used to calculate the degree of functionalization.

Infrared spectroscopy: The IR measurements were performed on a PerkinElmer FT-IR Spectrometer Frontier (Waltham, Massachusetts, USA). Spectra were recorded from 4000 to 650 cm^{-1} with a resolution of 4 cm^{-1}. Baseline correction and normalization was performed with the software Spectragryph 1.2.11.

Solid-state nuclear magnetic resonance (NMR) spectroscopy: Solid state NMR experiments were measured on a Bruker Avance III HD 400 spectrometer (resonance frequency of ^{1}H of 400.13 MHz, and ^{13}C of 100.61 MHz, respectively), equipped with a 4 mm dual broadband CP-MAS probe. ^{13}C spectra were obtained by using the TOSS (total sideband suppression) sequence at ambient temperature with a spinning rate of 5000 Hz. The NMR experiment was conducted with a cross-polarization (CP) contact

time of 2 ms, a recycle delay of 2 s, a SPINAL-64 ^{1}H decoupling and an acquisition time of 49 ms. The spectral width was set to 250 ppm. Chemical shifts were referenced externally against the carbonyl signal of glycine at δ = 176.03 ppm. The acquired FIDs were apodised with an exponential function (lb = 11 Hz) prior to Fourier transformation. All materials for solid-state NMR were soaked in deionized water as described by Zuckerstätter *et al.* before measurement.[2] For standard data processing the software Bruker TopSpin 3.5 was used. The crystallinity were determined by deconvolution of the crystalline and amorphous part of C4.[3] This method was used to estimate the effect of reaction conditions on the crystallinity of the samples. Peak fitting of native cellulose solid-state NMR spectrum was done according to Wickholm *et al*.[3] using the program Dmfit[4] and the elementary fibril diameter was calculated based on the work of Newman[5] using the average of the lateral cellulose chain spacings calculated from the 24 chain model (**Figure 2e** and **Figure S5**).[6] The resulting data from the fittings was used further to calculate as well the amount of hemicellulose in the sample and the crystallinity index in **Figure 2e**.

Gel permeation chromatography (GPC): For the GPC analysis approximately 15 mg (dry equivalent) of never-dried pulp samples were dispersed in 250 mL DI water and treated for approximately 20 s in a blender. One succinylated sample was treated with 4 mL of an aqueous NaOH solution (0.1 M) for 24 h. Throughout this treatment the sample was kept on a laboratory shaker. Then, the sample was rinsed with deionized water over a Büchner-funnel until the filtrate had a neutral pH (measured with indicator paper) and afterwards, it was washed with ethanol. The other samples were filtered and washed with ethanol. Each sample was transferred in a 4 mL vial, 4 mL of *N,N*-dimethylacetamide (DMAc) was added and the suspension was shaken overnight. Afterwards, the excess of DMAc was removed by filtration and 2 mL of DMAc/LiCl (9%, w/v) were added and shaken at room temperature until complete dissolution of the cellulose sample. Finally, 0.3 mL of the sample were diluted with 0.9 mL DMAc and filtered through a 0.45 µm grid syringe filter.

The GPC measurements were done with a multiple-angle laser light scattering (MALLS) detector with an argon ion laser (λ = 488 nm) (Wyatt Dawn DSP, Wyatt Inc. Santa Barbara, USA) and a refractive index (RI) detector (Shodex RI-71, Showa Denko K.K., Japan). Of every sample 100 µL were injected with an Agilent HP series 1100 autosampler (Agilent, Waldbronn, Germany). A Bio-Inert 1260 Infinity II (Agilent,

Waldbronn, Germany) was used and four serial GPC columns (Agilent PLgel Mixed ALS, 20 µm, 300 mm x 7.5 mm) were part of the system. The eluent was DMAc/LiCl (0.9%, w/v) at a flow rate of 1 mL/min and the run time was 45 min. The data was evaluated with Astra 4.7 and GRAMS/AI 7.0 software.

Solution-state NMR: To prepare the samples for NMR analysis, typically 50 mg of dried cellulosic material was added to a sealable sample vial and made up to 1 g by addition of stock $[P_{4444}][OAc]$:DMSO-d_6 (20:80 wt%) electrolyte solution.[7,8] The samples were magnetically stirred at room temperature until they went visually clear, which typically took ~1 hour. If the samples did not go clear during that period, the temperature was increased to 65 °C and when dissolved – transferred while hot into Wilmad 5 mm high-throughput tubes. All NMR runs were recorded on a Bruker AVANCE NEO 600 MHz spectrometer equipped with a 5-mm SmartProbe^{TM} set to 65 °C.

The diffusion-edited ^{1}H experiment used a 1D bipolar-pulse pair with stimulated echo (BPPSTE)[9] diffusion-ordered spectroscopy (DOSY) pulse sequence (Bruker pulse program 'ledbpgp2s1d'), with 3 s relaxation delay (d1), 0.5 s acquisition time (aq), 16 dummy scans (ds), 128 transient scans (ns), a sweep-width (sw) of 20 ppm with the transmitter offset on 6.1 ppm (o1p), diffusion time (d20) of 200 ms, gradient recovery delay (d16) of 0.2 ms, eddy current delay (d21) of 5 ms, diffusion gradient pulse duration (p30) of 2.5 ms, and z-gradient strength (gpz6) of 90% at ^{3} 50 G/cm (probe z-gradient strength). These conditions are specific to the NMR apparatus above and may need reoptimization for other systems. The diffusion-edited ^{1}H spectra for the sample of C6SA-cellulose is shown in (Figure S3a, b; upper trace of 2D spectra). The degree of substitution was determined from peak fitting of the ^{1}H-NMR C6SA-cellulose spectrum relating the protons from the glucose monomer unit to the protons of the succinyl group, respectively.

The HSQC experiments used a multiplicity-edited phase sensitive HSQC sequence with echo/antiecho-TPPI gradient selection (Bruker pulse program 'hsqcedetgp').[10] The parameters were as follows: spectral widths were 13 ppm and 165 ppm, with transmitter offsets (o1p) of 6.18 and 75 ppm, for ^{1}H and ^{13}C dimensions, respectively. The time-domain size (td1) in the indirectly detected ^{13}C-dimension (f1) was 512, corresponding to 256 t1-increments for the real spectrum. There were 16 dummy scans and 64 scans, an acquisition time of 0.065 s for f2 and a relaxation delay of 1.5

s. Sine squared (90°) window functions were used in f1 and f2. HSQC spectrum of the succinylated C6SA-cellulose is shown in Figure S3.
The regioselectivity of the succinylation was determined by peak fitting of the ^{1}H-NMR spectrum, according to a previously published work.[11]

Atomic Force Microscopy: AFM micrographs were obtained on a Cypher AFM using a Herzian TS-150 active vibration table and an ARC2 SPM controller. Tapping mode was used at 1 Hz using Tap-300-G cantilevers (nominal radius of curvature 8nm). The samples were prepared by first adsorbing poly(L-lysine) at pH 7 on freshly cleaved mica followed by thoroughly rinsing with deionized water. A sessile drop of 50 µL of CNF-SA suspension at 0.04% in water was spread over 1 cm^2. After 10-30 s, the samples were thoroughly rinsed with deionized water and imaged in water without intermediate drying.

Preparation of Aerogels:

Aerogels were prepared from C6SA-CNF hydrogels, which were either prepared by acidic treatment in 0.01 M HCl or basic treatment in 0.1 M NaOH. Both treatments induced a crosslinking, either by protonation of the sodium carboxylate groups or through saponification (removal of succinate esters). The prepared hydrogels were then solvent-exchanged to acetone: First solvent-exchange was conducted with acetone:water (1:1, v:v) for at least 12 h, then the hydrogels were equilibrated in pure acetone (3 times, each for at least 12 h). In all cases, the volume of the solvent used for exchange was approx. 10 times higher than the one of the hydrogels. The solvogels were then dried in a Leica EM CPD300 critical point dryer and the acetone was replaced with supercritical CO_2 over 25 cycles at 35 °C and 75 bar.

Scanning Electron Microscopy: SEM micrographs were obtained using a field emission scanning electron microscope (FE-SEM, Zeiss SigmaVP, Germany) operating at 1.6 kV and at a working distance of ca. 5 mm. The samples were sputter-coated with a 5 nm layer of platinum/palladium alloy prior to imaging.

Preparation of Films:

The nanofibrillated suspensions of TO-CNF nanocellulose and C6SA-CNF at 0.2 wt% were diluted to a 0.1% solid content by the addition of DI water and mixed in a magnetic stirrer (12 hours, 700 rpm). Before filtration, each sample was sonicated three times

(30% amplitude, 5 min) using a digital sonicator (Branson Ultrasonics Sonifier™ S-250D Digital Ultrasonic Cell Disruptor/Homogenizer). The filtration was carried using a pressurized air system (4 bar, 16h) in a self-made filtration device (**Figure S12**) consisitng of a tripod chamber (inner diameter of 12 cm, height 8.5 cm). The filtering medium was composed of one layer of polyvinylidene fluoride (PVDF) membrane filter (Durapore®, 142 mm diameter, 0.22 µm pore size, REF GVWP14250, Merck Millipore©), and a Schleicher & Schüll Rundfilter (150 mm diameter, Whatman™, Ref. No. 300212) underneath.

A hydrogel-like cake was obtained through filtration, and this cake was hot pressed using a series of covering layers at each side of the hydrogel cake for an optimal drying process. These covering layers are composed of a PVDF membrane filter (the same used on the filtration step), one layer of SEFAR NITEX® fabric, code: 03-1/1, four layers of regular bond paper, and three layers of strawboard, and finally an aluminum plate. The layer configuration and other characteristics of the system are presented in **Figure S12**.

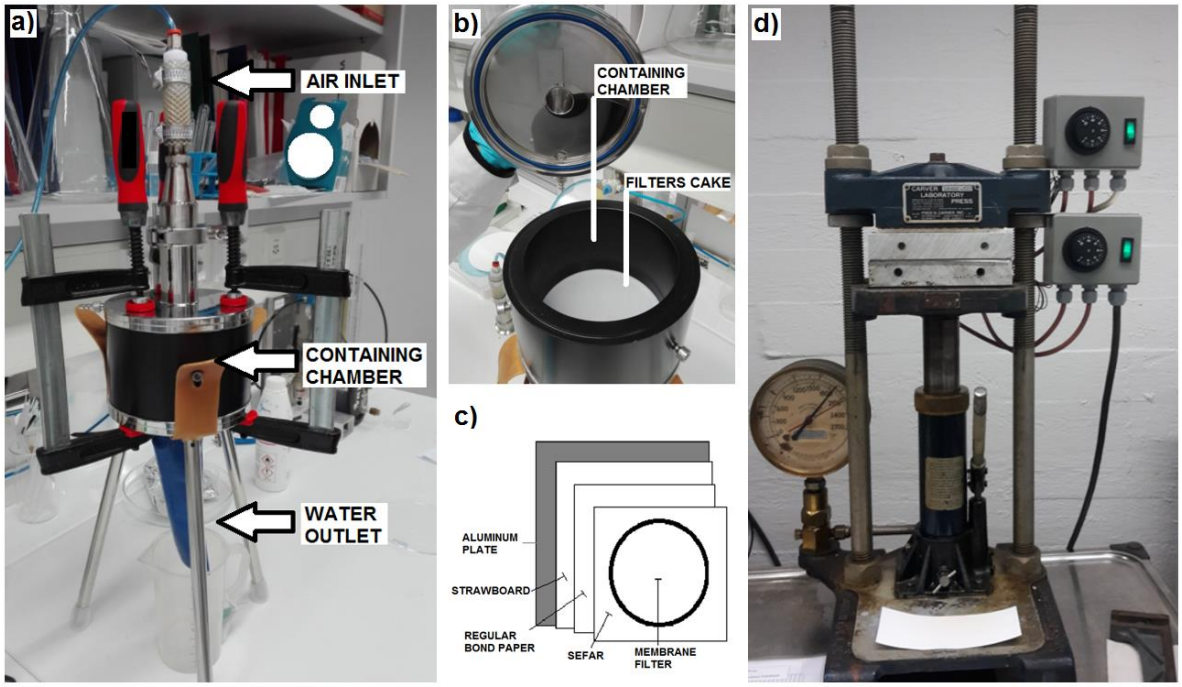

Figure S12. Films synthesis equipment. a) Vacuum filtration equipment, b) filtration containing chamber detailed, c) hot press layers disposition, d) hot press equipment

The hydrogel cakes with the protecting layers were hot-pressed in a Carver Laboratory Press 18200-213 (**Figure S12C-D**) (Freds Carver Inc. Hydraulic equipment, NJ, USA) at 1500 lb and 80 °C for 50 min. The prepared circular films had a diameter of 120 mm and thickness of approx. 50 μm.

Mechanical Characterization:

The mechanical properties of the films were evaluated using a Universal Tensile Tester Instron 4204 with 1 kN load cell at a test speed of 20 mm/min. The specimens for testing were prepared according to the ASTM D638-03 standard. The dry samples were stored before the test in a conditioned room at 50 % relative humidity and 23 °C for 48 h. The dry films were tested without any additional treatment, whereas the wet samples were immersed in the respective solutions: DI water, 0.01 M HCl (acidic treatment), and 0.1 M NaOH (basic treatment). After acidic and basic treatment, the wet films were equilibrated in DI water to remove salts.

The sample tests were carried out on pre-cut strips 5.3 mm x 30 mm and fixed to the Instron clamps, using sandpaper glued to the Instron clamps with UHU® removable adhesive putty. The thickness of the samples was measured using a micrometer (Mitutoyo Quickmike Series 293-IP-54, resolution 1 μm, EU). The mechanical test was repeated for each sample ten times; after eliminating the wrong test (slippery or wrong placed sample), at least six replicas of each sample were taken for the statistical analysis, and the results were averaged.

References

(1) Saito, T.; Hirota, M.; Tamura, N.; Kimura, S.; Fukuzumi, H.; Heux, L.; Isogai, A. Individualization of Nano-Sized Plant Cellulose Fibrils by Direct Surface Carboxylation Using TEMPO Catalyst under Neutral Conditions. *Biomacromolecules* **2009**, *10* (7), 1992–1996. https://doi.org/10.1021/bm900414t.

(2) Zuckerstätter, G.; Terinte, N.; Sixta, H.; Schuster, K. C. Novel Insight into Cellulose Supramolecular Structure through 13C CP-MAS NMR Spectroscopy and Paramagnetic Relaxation Enhancement. *Carbohydr. Polym.* **2013**, *93* (1), 122–128. https://doi.org/10.1016/j.carbpol.2012.05.019.

(3) Wickholm, K.; Larsson, P. T.; Iversen, T. Assignment of Non-Crystalline Forms in Cellulose I by CP/MAS 13C NMR Spectroscopy. *Carbohydr. Res.* **1998**, *312* (3), 123–129. https://doi.org/10.1016/S0008-6215(98)00236-5.

(4) Massiot, D.; Fayon, F.; Capron, M.; King, I.; Le Calvé, S.; Alonso, B.; Durand, J.-O.; Bujoli, B.; Gan, Z.; Hoatson, G. Modelling One- and Two-Dimensional Solid-State NMR Spectra. *Magn. Reson. Chem.* **2002**, *40* (1), 70–76. https://doi.org/10.1002/mrc.984.

(5) Newman, R. H. Estimation of the Lateral Dimensions of Cellulose Crystallites Using 13C NMR Signal Strengths. *Solid State Nucl. Magn. Reson.* **1999**, *15* (1), 21–29. https://doi.org/10.1016/S0926-2040(99)00043-0.

(6) Oehme, D. P.; Downton, M. T.; Doblin, M. S.; Wagner, J.; Gidley, M. J.; Bacic, A. Unique Aspects of the Structure and Dynamics of Elementary Iβ Cellulose Microfibrils Revealed by Computational Simulations. *Plant Physiol.* **2015**, *168* (1), 3–17. https://doi.org/10.1104/pp.114.254664.

(7) Koso, T.; Rico del Cerro, D.; Heikkinen, S.; Nypelö, T.; Buffiere, J.; Perea-Buceta, J. E.; Potthast, A.; Rosenau, T.; Heikkinen, H.; Maaheimo, H.; Isogai, A.; Kilpeläinen, I.; King, A. W. T. 2D Assignment and Quantitative Analysis of Cellulose and Oxidized Celluloses Using Solution-State NMR Spectroscopy. *Cellulose* **2020**, *27* (14), 7929–7953. https://doi.org/10.1007/s10570-020-03317-0.

(8) King, A. W. T.; Mäkelä, V.; Kedzior, S. A.; Laaksonen, T.; Partl, G. J.; Heikkinen, S.; Koskela, H.; Heikkinen, H. A.; Holding, A. J.; Cranston, E. D.; Kilpeläinen, I. Liquid-State NMR Analysis of Nanocelluloses. *Biomacromolecules* **2018**, *19* (7), 2708–2720. https://doi.org/10.1021/acs.biomac.8b00295.

(9) Wu, D. H.; Chen, A. D.; Johnson, C. S. An Improved Diffusion-Ordered Spectroscopy Experiment Incorporating Bipolar-Gradient Pulses. *J. Magn. Reson. A* **1995**, *115* (2), 260–264. https://doi.org/10.1006/jmra.1995.1176.

(10) Willker, W.; Leibfritz, D.; Kerssebaum, R.; Bermel, W. Gradient Selection in Inverse Heteronuclear Correlation Spectroscopy. *Magn. Reson. Chem.* **1993**, *31* (3), 287–292. https://doi.org/10.1002/mrc.1260310315.

(11) Beaumont, M.; Jusner, P.; Gierlinger, N.; W. T. King, A.; Potthast, A.; Rojas, O. J.; Rosenau, T. Unique Reactivity of Nanoporous Cellulosic Materials Mediated by Surface-Confined Water. *Nat. Commun.* **2021**, *12*, 2513. https://doi.org/10.1038/s41467-021-22682-3.

(12) Okita, Y.; Saito, T.; Isogai, A. Entire Surface Oxidation of Various Cellulose Microfibrils by TEMPO-Mediated Oxidation. *Biomacromolecules* **2010**, *11* (6), 1696–1700. https://doi.org/10.1021/bm100214b.